MODELLING OF LIGHTNING STRIKE DAMAGE OF CFRP LAMINATES CAUSED BY SUDDEN SURFACE PLASMA EXPANSION

Kunkun Fu[1], Lin Ye[1], Li Chang[1] and Chunhui Yang[2]

[1]School of Aerospace, Mechanical and Mechatronic Engineering, the University of Sydney
NSW 2006, Australia
kunkun.fu@sydney.edu.au, lin.ye@sydney.edu.au, li.chang@sydney.edu.au
[2]School of Computing, Engineering and Mathematics, Western Sydney University
NSW 2751, Australia
r.yang@westernsydney.edu.au

Keywords: Lightning strike damage, CFRP laminates, Plasma explosion, Finite element modelling

ABSTRACT

Carbon fibre reinforced plastics (CFRP) composites have been widely used in modern airplanes due to their high strength-weight ratio and high stiffness-weight ratio in performance. However, the use of CFRP composites poses a risk of lightning strike damage even when surface protection systems were used. In this work, a finite element (FE) model was presented to predict the mechanical damage in a CFRP laminate caused by the surface plasma expansion. The plasma arc radius together with the pressure pulse was determined by a surface explosion model. Then, the pressure pulse was applied in the FE model to determine the impact behaviour and failure mechanisms in the CFRP laminate, such as intra-laminar damage and inter-laminar delamination. It is found that a 200 kA lightning current can induce a pressure magnitude up to 158 MPa. The highest deflection and velocity occurs at the centre of the bottom ply were 9.72 mm and 317.4 m/s, respectively. In addition, the severe interlaminar delamination and intra-laminar damage were found in the bottom plies.

1 INTRODUCTION

Carbon fibre reinforced plastics (CFRP) composites are increasingly used to replace the conventional metal alloys in aerospace, marine and transportation industries due to their high strength-weight ratio and high stiffness-weight ratio in performance. However, the use of semi-conductive CFRP composites in a modern airplane presents a lightning strike threat to the flight safety. Compared to metallic counterparts, CFRP composites show a much lower electrical conductivity, which may not readily conduct away a high lightning current. Thus, the lightning may causes intensive resistive heating in the CFRP composites leading to severe ablation damage such as pyrolysis of polymer matrices and burning of carbon fibres. To prevent the damage to a CFRP composite, a lightning strike protection (LSP) system has been attached to the composite surface to conduct away the high lightning current. According to some existing experimental results [1-4], the protecting layer was vaporized when a high current is applied, and high-temperature plasma creates a pressure pulse in CFRP composites. Therefore, quantitative characterisation of the sudden surface plasma expansion allows accurate assessment of damage in CFRP composites during a lightning strike.

To date, some experimental studies [5-7] have been presented to understand the damage of pristine CFRP laminates. For instance, *Hirano et al*. [5] experimentally examine the damage evolution in unidirectional CFRP composites under an artificial lightning strike test. *Li et al.* [6] performed the lightning strike experiments on carbon woven fabric/epoxy laminates with two stacking sequence, and they found that lay-up sequence has a great effect on the lightning strike damage to the laminates. *Feraboli et al.* [7] investigated the residual strength and modulus of unnotched and filled-hole CFRP laminates in tension and compression after simulated lightning strike tests. In addition, it has been reported that the damage can still exist in CFRP laminates with protections due to the poor design of the protection system [1, 3]. Compared to the simulated lightning strike experiments, numerical modelings [4-6] can quantitatively predict the lightning strike damage with significantly fewer costs

describing lightning strike mechanisms of CFRP laminates with and without the protection. Ogasawara et al. [8] predicted the lightning strike damage in CFRP composites using a coupled electrical-thermal finite element (FE) analysis. *Abdelal et al.* [9] presented an FE model considering the temperature-dependent materials properties to estimate the lightning strike damage. *Wang et al.* [10] numerically obtained the ablation damage of CFRP composites during a lightning strike and predicted the residual strength after a lightning strike. *Fu et al.* [11] developed a coupled thermal-electrical model to determine the damage in CFRP laminates with an advanced LSP system. The lightning protection mechanisms were discussed from the aspect of Joule heating-induced damage. Most of the numerical models have focused on the transition of lightning electricity and Joule heating in CFRP laminates during a lightning strike event. There is little effort [12-14] so far to quantify the damage caused by the dynamic stresses induced by a lightning strike. *Lepetit et al.* [12] proposed a surface explosion model to determine the pressure pulse caused by lightning strike. *Muñoz et al.* [13] presented an FE model considering electromagnetic/acoustic pressure to address the mechanical effects of the lightning strike on CFRP laminates. *Liu et al.* [14] proposed a combing electrical-thermal FE analysis and blow-off impulse analysis to investigate lightning strike effects on damage behaviour of composite.

This work aims to develop a systematic FE model to predict the mechanical damage in CFRP laminates with the full electrical-thermal protection, caused by the surface plasma explosion. First, a surface plasma explosion model was developed. Then, a dynamic mechanistic FE model was established considering the failure behaviour such as intra-laminar damage, interlaminar and adhesive delamination of the CFRP laminates. The FE model was used to predict the dynamic response and mechanical damage in a CFRP laminate with the protection.

2 THEORY

2.1 Lightning current

A lighting event is associated with a high lightning current. Recently, a standard has been published to describe the current waveform for an airplane as shown in Figure 1a. It is seen that the current has been categorized as four components. Component A is an initial stroke with a peak amplitude of 200 kA with a less than 500 us. Component D is a lightning restrike with a peak amplitude of 100 kA with a less than 500 us duration. Component A is an extreme case for an airplane, which is usually simplified as a double exponential curve as follows,

$$I(t) = kI_{peak}(e^{-\alpha t} - e^{-\beta t}) \tag{1}$$

where I_{peak} is the peak amplitude of the current. α, β, k are constants defining the shape of the current waveform. T1 and T2 are front time and tail time respectively, which are commonly used to define the waveform as shown in Figure 1b.

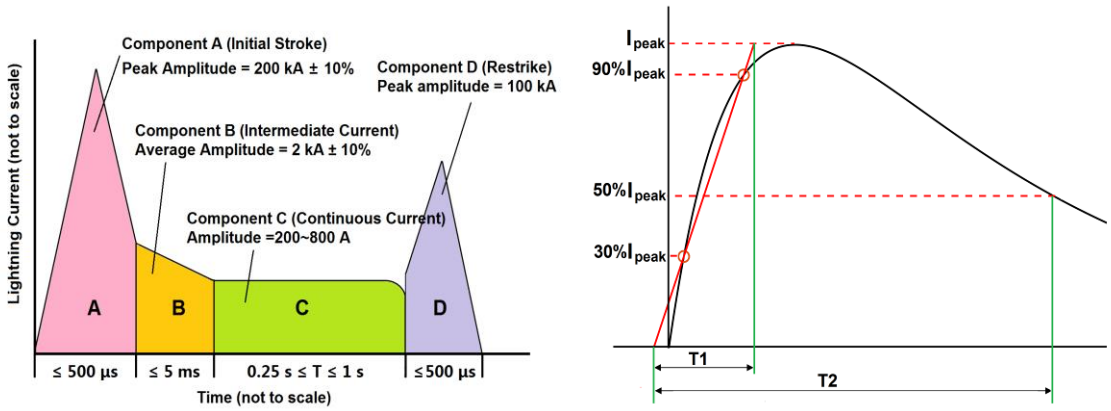

(a) (b)

Figure 1 (a) Schematic lightning current waveform and (b) parameters definition, modified from [15]

2.2 Plasma channel radius

It is reported [16] that a moderate thunderstorm can produce up to several hundred megawatts of electrical power. When the high-energy lightning pulse is applied onto the CFRP laminates, the surface is vaporized in a very short duration and is transformed into plasma by ionisation. High-temperature plasma creates a pressure pulse to the laminates. Accordingly, a shock wave is produced inside the materials, leading to the potential mechanical damage to the laminates. The mechanical damage is more severe if the plasma is confined by the protecting layer on top of the laminates. Plasma channel radius can be calculated using the following equation by Braginskii [17],

$$R(t) = \lambda \rho_a^{-1/6} \left[I(t) \right]^{1/3} t^{1/2} \tag{1}$$

where λ is a constant, λ =0.294 in [17]. Recently, Cooray and Rahman [18] found that λ =0.102 gives a better radius prediction with experimental data. Thus, λ =0.102 is adopted in our study. ρ_a is air density at atmosphere pressure, ρ_a=1.29 kg/m^3. Using Eq. 1, plasma channel radius is predicted with a T1/T2=2.6 μs/50 μs with different I_{peak} as illustrated in Figure 2. Plasma channel radius expands with the time.

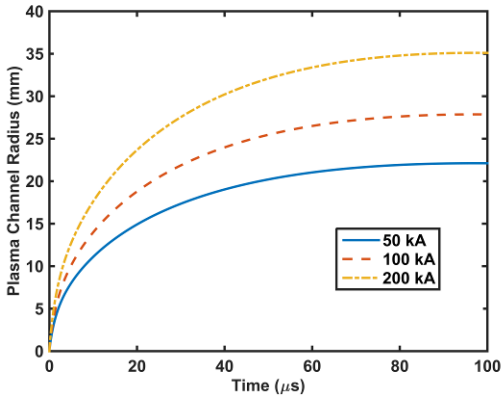

Figure 2 Plasma channel radius caused by a current waveform T1/T2=2.6 μs/50 μs

2.2 Surface explosion model

A surface explosion model to determine the pressure pulse by high-energy laser has been developed by Fabbro et al. [19] and has been adopted to predict the pressure due to a lightning strike by Lepetit et al. [12]. For the protected CFRP laminates, the relation between the time-dependent pressure pulse P(t) and the gap distance L(t) can be determined by the following equation,

$$\frac{d^2 L(t)}{dt^2} = \left(\frac{1}{\mu_p} + \frac{1}{\mu_c} \right) P(t) \tag{1}$$

where μ_p and μ_c are the mass per unit area of protecting layer and CFRP laminates. According to the energy conservation formula, the energy per unit area is consist of internal energy and the work by the pressure,

$$W(t) = P(t) \frac{dL}{dt} + \frac{d}{dt} \left(\frac{3}{2F} PL \right) \tag{2}$$

where F is a fraction of the internal energy to the thermal energy. $W(t)$ can be determined by the following equation,

$$W(t) = \frac{\left(1 + 4 \ln(\frac{r}{R(t)}) \right) Z_s I^2(t)}{8\pi^2 r^2} \tag{3}$$

where r is the effective radius where the pressure is applied. R is arc radius. Z_s is the electrical surface

impedance. Then, the numerical solution can be obtained by solving the Eqs. 1-3.

3 FINITE ELEMENT MODEL

3.1 Explicit FE models

In this study, an explicit FE model describing the mechanical damage of CFRP laminates, of full electrical-thermal protection, was developed using ABAQUS. In this case, transition of lightning electricity and Joule heating are not considered. A laminate with a lay-up sequence $[45°/0°/-45°/90°]_S$ is an 8-ply quasi-isotropic laminate was considered as a case study. Figure 3 shows the schematic of the FE mesh and the boundary condition. The dimension of the laminate is 450 mm×450 mm×1.5 mm, and fixed constraints were applied on four edges of the laminates. A cylindrical pressure pulse was applied to the centre of the laminates. The pressure is determined using the method specified in Section 2. After mesh sensitivity analysis, the FE model has 33056 four-node shell elements.

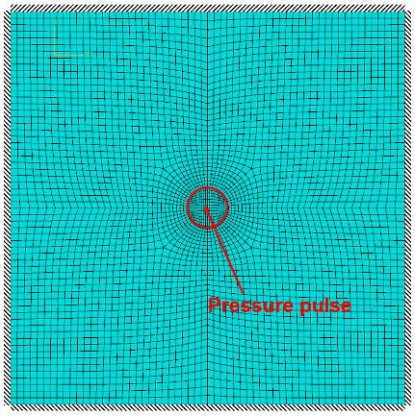

Figure 3 FE model and boundary conditions

3.2 Progressively intra-laminar damage model

Hashin criteria were used here to describe progressively the inter-laminar damage initiation and evolution of the CFRP laminates. Damage initiation represents the onset of the degradation of the materials with four failure modes, i.e. fibre tension, fibre compression, matrix tension, and matrix compression. The damage initiates when the following equations are met.

For the fibre tension when $\hat{\sigma}_{11} \geq 0$, we have

$$F_f^t = \left(\frac{\hat{\sigma}_{11}}{X^T}\right)^2 + \alpha\left(\frac{\hat{\tau}_{12}}{S^L}\right)^2 \tag{4}$$

Regarding the fibre compression when $\hat{\sigma}_{11} < 0$,

$$F_f^c = \left(\frac{\hat{\sigma}_{11}}{X^C}\right)^2 \tag{5}$$

For the matrix tension when $\hat{\sigma}_{22} \geq 0$,

$$F_m^t = \left(\frac{\hat{\sigma}_{22}}{Y^T}\right)^2 + \left(\frac{\hat{\tau}_{12}}{S^L}\right)^2 \tag{6}$$

Regarding the matrix compression when $\hat{\sigma}_{22} < 0$, we have

$$F_m^c = \left(\frac{\hat{\sigma}_{22}}{2S^T}\right)^2 + \left[\left(\frac{Y^C}{2S^T}\right)^2 - 1\right]\frac{\hat{\sigma}_{22}}{Y^C} + \left(\frac{\hat{\tau}_{12}}{S^L}\right)^2 \tag{7}$$

where X^T and X^C are the tensile and compressive strength in the longitudinal direction, Y^T and Y^C are the tensile and compressive strength in the transverse direction, S^L and S^T denote shear strength in the

longitudinal and transverse directions; $\hat{\sigma}_{11}$ and $\hat{\sigma}_{22}$ are the effective normal stress tensors and $\hat{\tau}_{12}$ is the shear stress tensor, α is a coefficient factor that reflects the contribution of shear stress to the fibre tensile mode, and it is set as 1.0 to fully consider the influence of shear stress; F is the assessment value that indicates, and if it is equal to or higher than 1, the damage initiation criteria are met, and the subsequent damage progression process will begin.

The damage is modulated by calculating equivalent stresses and strains in a linear degradation manner after the damage initiation occurs at any of the four failure modes:

Fibre tension ($\hat{\sigma}_{11} \geq 0$, $\varepsilon_{11} \geq 0$)

$$\delta_{eq}^{ft} = L^c \sqrt{\langle \varepsilon_{11} \rangle^2 + \alpha \varepsilon_{12}^2} \tag{8}$$

$$\sigma_{eq}^{ft} = \frac{\langle \sigma_{11} \rangle \langle \varepsilon_{11} \rangle + \alpha \tau_{12} \varepsilon_{12}}{\delta_{eq}^{ft} / L^c} \tag{9}$$

Fibre compression ($\hat{\sigma}_{11} < 0$, $\varepsilon_{11} < 0$)

$$\delta_{eq}^{fc} = L^c \langle -\varepsilon_{11} \rangle \quad \sigma_{eq}^{fc} = \frac{\langle -\sigma_{11} \rangle \langle -\varepsilon_{11} \rangle}{\delta_{eq}^{fc} / L^c} \tag{10}$$

Matrix tension ($\hat{\sigma}_{22} \geq 0$, $\varepsilon_{22} \geq 0$)

$$\delta_{eq}^{mt} = L^c \sqrt{\langle \varepsilon_{22} \rangle^2 + \varepsilon_{12}^2} \quad \sigma_{eq}^{mt} = \frac{\langle \sigma_{22} \rangle \langle \varepsilon_{22} \rangle + \tau_{12} \varepsilon_{12}}{\delta_{eq}^{mt} / L^c} \tag{11}$$

Matrix compression ($\hat{\sigma}_{22} < 0$, $\varepsilon_{22} < 0$)

$$\delta_{eq}^{mc} = L^c \sqrt{\langle -\varepsilon_{22} \rangle^2 + \varepsilon_{12}^2} \quad \sigma_{eq}^{mc} = \frac{\langle -\sigma_{22} \rangle \langle -\varepsilon_{22} \rangle + \tau_{12} \varepsilon_{12}}{\delta_{eq}^{mc} / L^c} \tag{12}$$

where L^c, the characteristic length, is based on the element geometry and introduced to normalize the elements with different sizes. The damage variable for a particular mode is given by,

$$d = \frac{\delta_{eq}^f (\delta_{eq} - \delta_{eq}^0)}{\delta_{eq}^0 (\delta_{eq}^f - \delta_{eq}^0)} \tag{13}$$

where δ^0_{eq} is the initial state at which the initiation criterion for that failure mode was met, and δ^f_{eq} is the state at which the material is completely damaged in this failure mode. The materials failed as long as the damage variable d associated with the fiber failure modes (tensile or compressive) reaches to one. The materials properties shown in Table 1 are selected from the works [20, 21].

Elastic properties [GPa]		Strength [MPa]		In-plane fracture toughness [J/m^2]	
E_1	153	X^T	2537	$G_{1C}{}^T$	9160
E_2	10.3	X^C	1580	$G_{1C}{}^C$	7990
G_{12}	10.3	Y^T	82	$G_{2C}{}^T$	220
G_{13}	6	Y^T	236	$G_{2C}{}^C$	1100
G_{23}	6	S^T	90		
V_{12}	0.3	S_C	40		

Table 1: Materials properties in CFRP composite for intra laminar damage model [20, 21]

3.3 Interlaminar delamination model

Interlaminar delamination between plies in composites was modelled using a cohesive zone method, and the behaviour of interlaminar degradation and failure were described by a traction-separation law. The fracture mechanisms involve a damage initiation criterion followed by a damage evolution law. In this work, the damage/delamination initiates when the following quadratic stress

criterion is satisfied,

$$\left\{\frac{\langle t_n \rangle}{t_n^0}\right\}^2 + \left\{\frac{\langle t_s \rangle}{t_s^0}\right\}^2 + \left\{\frac{\langle t_t \rangle}{t_t^0}\right\}^2 = 1 \tag{14}$$

where t_i (i=*n*,*s*,*t*) is defined as the nominal traction stress vector in the normal *n* and shear *s* and *t*, directions, respectively. t_i^0 (i=*n*,*s*,*t*) is the corresponding strength in normal *n* and shear *s* and *t* directions, respectively. The values of the strength of composite were selected from a numerical work [22].

The damage evolution law depicts the degradation of the cohesive stiffness once the initiation criterion is met. In this work, a linear softening relation was adopted to modulate the stiffness degradation from the damage initiation to the final failure. Benzeggagh-Kenane fracture criterion [22] was utilized to model the damage process as expressed by the following equation,

$$G_n^C + \left(G_s^C - G_n^C\right)\left\{\frac{G_S}{G_T}\right\}^\eta = G_C \tag{15}$$

where G_S=G_s+G_t, G_T=G_n+G_s, defined as the fracture toughness in the mode I (*n*) and Mode II (*s*) and III (*t*), respectively. G_C represents the total fracture toughness. η denotes the cohesive property parameter. η =1.45 was used here based on the experiment results [23]. The mechanical properties used are listed in Table 2.

	Mode I	Mode II	Mode III
Normalized elastic modulus [GPa]	2890	2890	2890
Interlaminar strength [MPa)	33	54	54
Interlaminar fracture toughness [J/m^2]	330	800	800

Table 2: Materials properties in CFRP composite for interlaminar damage model [22]

3 RESULTS AND DISCUSSION

Prior to the FE analysis, the lightning-induced pressure magnitude is obtained by the surface explosion model described in Section 2. Figure 4 shows the predicted pressures caused by a lightning current waveform T1/T2=2.6 μs/50 μs. It is found that the pressure waveforms are similar when different peak currents are utilized. The predicted pressure magnitude reaches their peak values in a very short time (less than 1 μs). After that, the pressure drop back to zero in ~100 μs. The 200 kA current (component A) induces the highest pressure amplitude of ~158 MPa, which is selected to investigate the mechanical damage in the protected CFRP laminate.

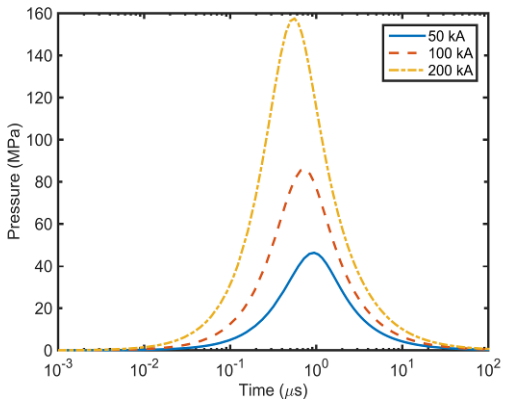

Figure 4 Pressure magnitude in the protected CFRP laminate by the surface explosion model

We apply the pressure predicted as above in the FE model. The deflection response of the CFRP laminate are examined. In the bottom surface, the centre and other four sampling points (of a distance

D) located in the same direction with an interval of 24 mm are chosen. In Figure 5a, the greatest deflection happens in the centre at ~48 μs, with a value of ~9.72 mm. After that, the deflection gradually decreases with the time. For the sampling locations points away from the centre, a pressure-induced shock wave propagation is found. The responses of the four sampling location are delayed at a same interval and their peak deflections decrease with the distance from the centre. The deflection caused by the wave propagation is high, and the shock wave propagation may induce damage in the laminate. In addition, the velocity of these five points in the bottom ply is also determined as illustrated in Figure 5b. It is found that the maximum velocity is 317.4 m/s happening at the time when the pressure pulse vanishes. For the other sampling location, the peak velocities decrease with an increase in the distance, D, indicating the occurrence of wave attenuation.

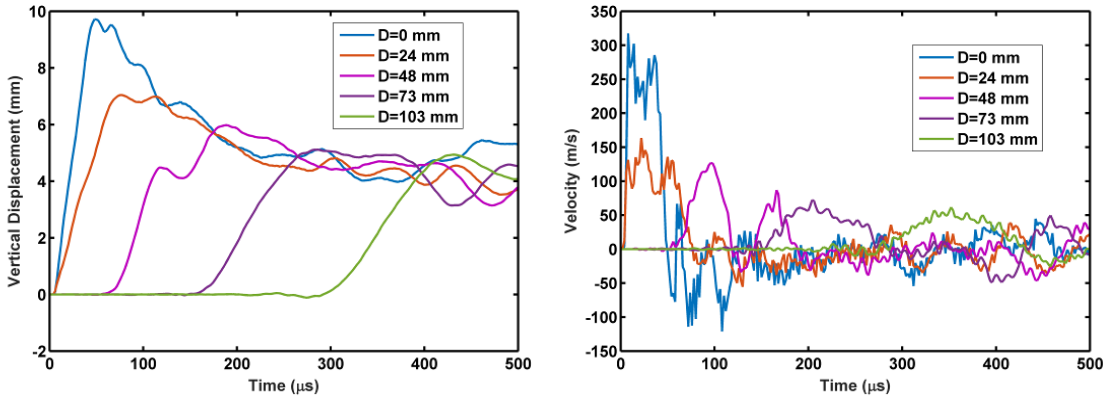

(a) (b)

Figure 5 Pressure in protected CFRP predicted by the surface explosion model

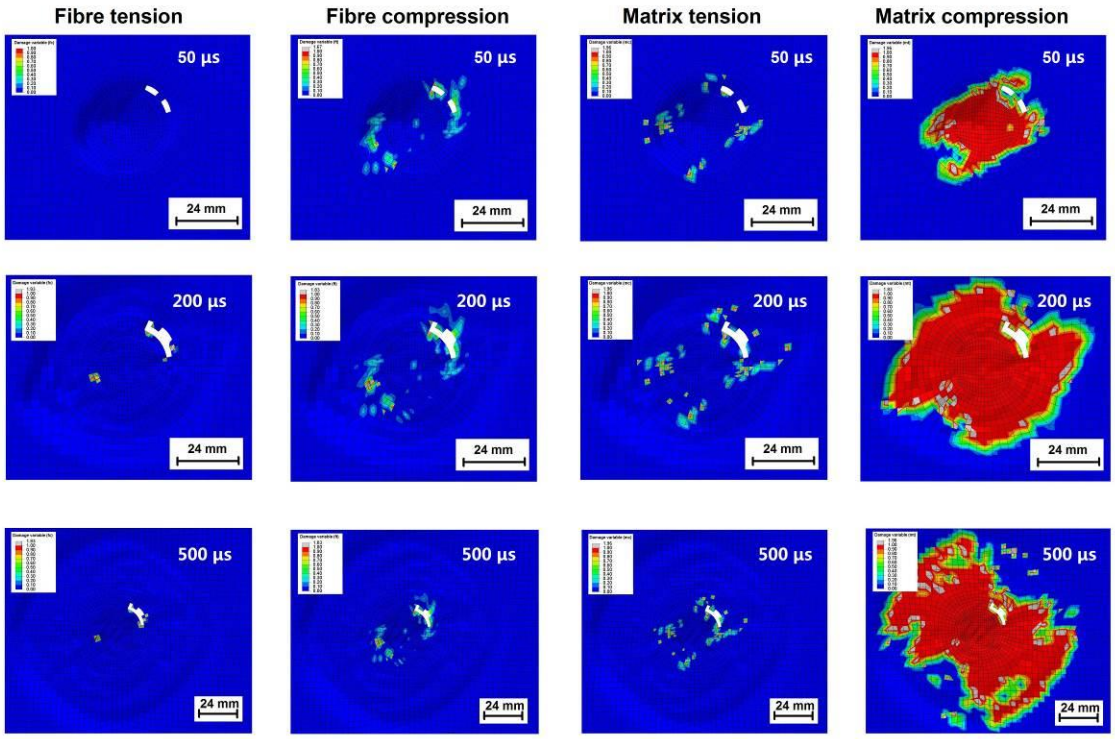

Figure 6 Damage variables in tension and compression of fibre and matrix at different time

Next, the intra-laminar damage and interlaminar delamination of the CFRP laminates are obtained. It is observed that the damage primarily happens in the bottom ply. In order to determine the failure modes and damage evolution, the damage variables are plotted at 50-500 μs as shown in Figure 6. It can be seen that the damage variables show a 45° orientation due to the fibre direction in this ply are 45°. At 50 μs, a few elements were fully damage and removed as the corresponding damage variables for compression reach one. Fibre damage in tension is not found, and therefore, the damage is mainly caused by the compression. In the meanwhile, the matrix damage is severe in the bottom ply. As the time increases, more elements are damage and removed due to the shock wave propagation at 200 μs and 500 μs. In addition, the area of matrix damage also increases.

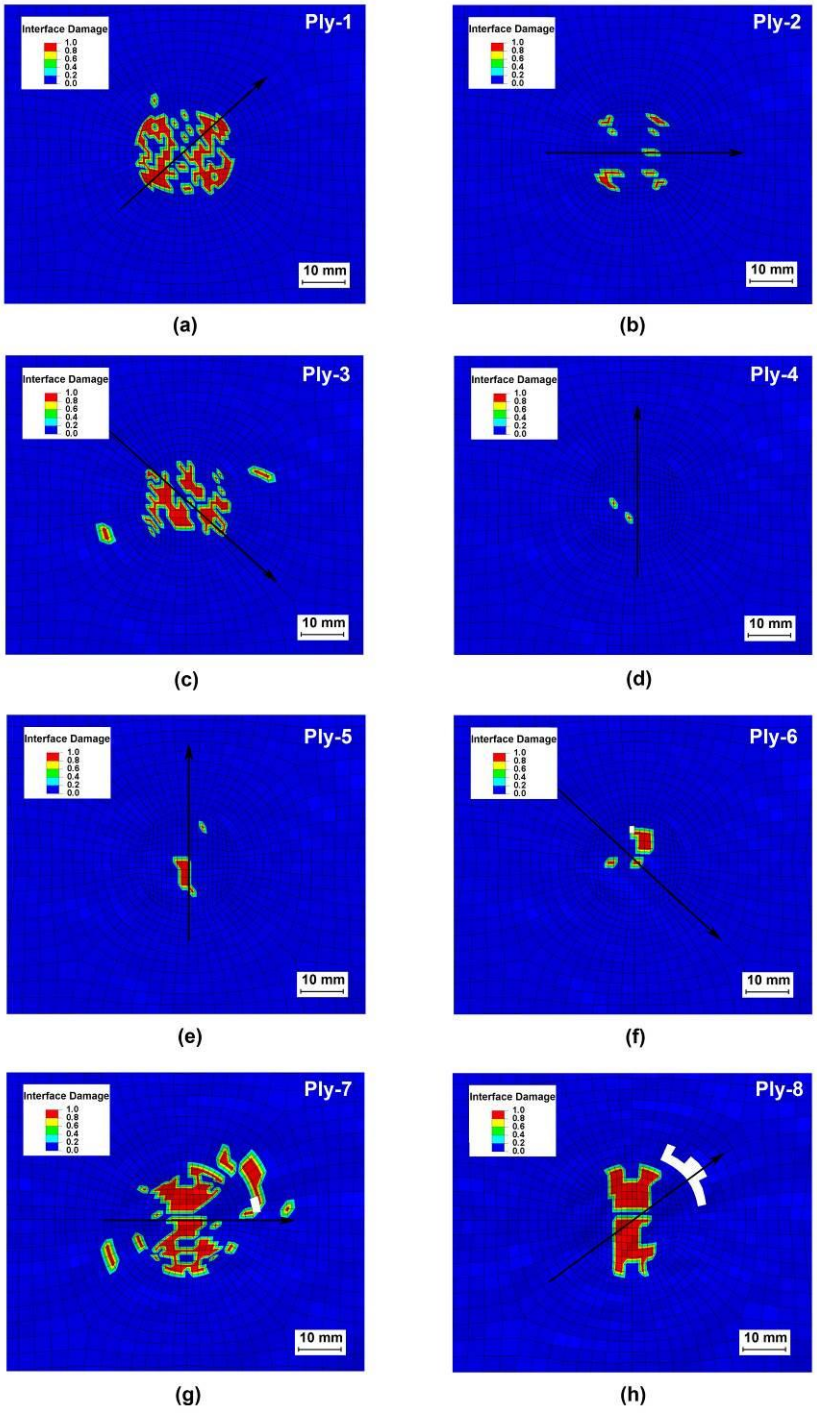

Figure 7 Delamination in (a) ply-1, (b) ply-2, (c) ply-3, (d) ply-4, (e) ply-5, (f) ply-6, (g) ply-7 and (h) ply-8 at 500 μs (arrows indicate the fibre orientation)

The delamination damage are determined at each ply. in each ply is examined as shown in Figure 7. It can be seen that the delamination occurs primarily in the top plies and the bottom two plies. The pressure pulse causes the bending of the laminate and thus the interface damage were induced. Unlike the intralaminar damage, interlaminar delamination is insensitive to the fibre orientation.

4 CONCLUSIONS

In this work, an FE model with a surface plasma explosion model has been developed to predict the mechanical damage in CFRP laminates with full electrical-thermal protection, caused by a lightning strike. The peak deflection was 9.72 mm and the maximum velocity reached up to 317.4 m/s for a lightning strike with a peak current of 200 kA. In addition, severe delamination and intralaminar damage were found in an 8-ply quasi-isotropic CFRP laminate in a case study. This result indicates mechanical damage cannot be neglected when a lightning protection system is developed for a CFRP laminate.

ACKNOWLEDGEMENTS

The authors are grateful for a Discovery Project (DP150100531) from Australian Research Council.

REFERENCES

[1] J.H. Han, H. Zhang, M.J. Chen, D. Wang, Q. Liu, Q.L. Wu, Z. Zhang, The combination of carbon nanotube buckypaper and insulating adhesive for lightning strike protection of the carbon fiber/epoxy laminates, *Carbon*, **94**, 2015, pp. 101-113 (doi: 10.1016/j.carbon.2015.06.026)

[2] B. Lepetit, F. Soulas, S. Guinard, Y. Duval, I. Revel, G. Peres, Analysis of composite panel damages due to a lightning strike : mechanical effects, *Proceedings of International Conference on Lightning Static Electricity, Oxford, UK, September 6-8, 2011*

[3] F.S. Wang, Y.Y. Ji, X.S. Yu, H. Chen, Z.F. Yue, Ablation damage assessment of aircraft carbon fiber/epoxy composite and its protection structures suffered from lightning strike, *Composite Structures*, **145**, 2016, pp. 226-241 (doi: 10.1016/j.compstruct.2016.03.005)

[4] J.M. Welch. Repair design, test, and process considerations for lightning strikes. *Proceedings of Joint FAA-Boeing-Airbus Damage Tolerance Workshop, Amsterdam, Netherlands, 2007*

[5] Y. Hirano, S. Katsumata, Y. Iwahori and A. Todoroki, Artificial lightning testing on graphite/epoxy composite laminate, *Composites Part A: Applied Science and Manufacturing*, **41**, 2010, pp. 1461-1470 (doi: 10.1016/j.compositesa.2010.06.008)

[6] Y. Li, R. Li, L. Lu, X. Huang, Experimental study of damage characteristics of carbon woven fabric/epoxy laminates subjected to lightning strike, *Composites Part A: Applied Science and Manufacturing*, **79**, 2015, pp. 164-175 (doi: 10.1016/j.compositesa.2015.09.019)

[7] P. Feraboli and M. Miller, Damage resistance and tolerance of carbon/epoxy composite coupons subjected to simulated lightning strike, *Composites Part A: Applied Science and Manufacturing*, **40**, 2009, pp. 954-967 (doi: 10.1016/j.compositesa.2009.04.025)

[8] T. Ogasawara, Y. Hirano and A. Yoshimura, Coupled thermal-electrical analysis for carbon fiber/epoxy composites exposed to simulated lightning current, *Composites Part A: Applied Science and Manufacturing*, **41**, 2010, pp. 973-981 (doi: 10.1016/j.compositesa.2010.04.001)

[9] G. Abdelal, and A. Murphy, Nonlinear numerical modelling of lightning strike effect on composite panels with temperature dependent material properties, *Composite Structures*, **109**, 2014, pp. 268-278 (doi: 10.1016/j.compstruct.2013.11.007)

[10] F.S. Wang, N. Ding, Z.Q. Liu, Y.Y. Ji, and Z.F. Yue, Ablation damage characteristic and residual strength prediction of carbon fiber/epoxy composite suffered from lightning strike. *Composite Structures*, **117**, 2014, pp. 222-233 (doi: 10.1016/j.compstruct.2014.06.029)

[11] K.K. Fu, L. Ye, L. Chang, C.H. Yang, Z. Zhong, Modelling of lightning strike damage to CFRP composites with an advanced protection system. Part I: thermal–electrical transition, *Composite Structures*, **165**, 2017, pp. 83-90 (doi: 10.1016/j.compstruct.2017.01.008)

[12] B. Lepetit, C. Escure, S. Guinard, I. Revel, G. Peres, Thermo-mechanical effects induced by lightning on carbon fiber composite materials. *Proceedings of International Conference on Lightning Static Electricity*, Oxford, UK, September 6-8, 2011

[13] R. Muñoz, S. Delgado, C. González, B. López-Romano, D. Wang, J. LLorca, Modeling lightning impact thermo-mechanical damage on composite materials, *Applied Composite Materials*, **21**, 2014 pp. 149-164 (doi: 10.1007/s10443-013-9377-9)

[14] Z.Q. Liu, Z.F. Yue, F.S. Wang, Y.Y. Ji, Combining analysis of coupled electrical-thermal and blow-off impulse effects on composite laminate induced by lightning strike, *Applied Composite Materials*, **22**, 2015, pp. 189-207 (doi: 10.1007/s10443-014-9401-8)

[15] Standard, Lightning qualification test techniques for aerospace vehicles and hardware, *MIL-STD-1757*, 1983

[16] E.R. Williams. The electrification of thunderstorms. *Scientific American*, **259**, 1988, pp. 88-99

[17] S. Braginskii, Theory of the development of a spark channel, *Soviet Physics JETP*, **34**, 1958, pp. 1068-1074

[18] C. Vernon, R. Mahbubur, On the relationship between the discharge current, energy dissipation and the NO_x production in spark discharges, *Proceedings of International Conference on Lightning and Static Electricity, Seattle, USA, 19-23 September, 2005*

[19] R. Fabbro, J. Fournier, P. Ballard, D. Devaux, J. Virmont, Physical study of laser-produced plasma in confined geometry, *Journal of Applied Physics*, **68**, 1990, pp. 775-784 (doi: 10.1063/1.346783)

[20] A. Faggiani, B.G. Falzon BG, Predicting low-velocity impact damage on a stiffened composite panel, *Composites Part A: Applied Science and Manufacturing*, **41**, 2010, pp. 737–49 (doi: 10.1016/j.compositesa.2010.02.005)

[21] A. Jumahat, C. Soutis, A. Hodzic. A graphical method predicting the compressive strength of toughened unidirectional composite laminates, *Applied Composite Materials*, **18**, 2011, pp. 65–83 (doi: 10.1007/s10443-010-9149-8)

[22] A. Qiu, K. Fu, W. Lin, C. Zhao, Y. Tang, Modelling low-speed drop-weight impact on composite laminates, *Materials & Design*, **60**, 2014, pp. 520-531 (doi: 10.1016/j.matdes.2014.04.041)

[23] P.P. Camanho, C.G. Davila, Mixed-mode decohesion finite elements for the simulation of delamination in composite materials, *Technique Report, NASA/TM-2002-211737*, 2002